Optics Communications 459 (2020) 124948

Contents lists available at ScienceDirect

Optics Communications

journal homepage: www.elsevier.com/locate/optcom

Ultra-broadband metamaterial absorber in long wavelength Infrared band based on resonant cavity modes

Yi Luo [a,b], Dejia Meng [a], Zhongzhu Liang [a,*], Jin Tao [a], Jingqiu Liang [a], Changhong Chen [c], Jianjun Lai [c], Tarik Bourouina [d], Yuxin Qin [a], Jinguang Lv [a], Yuhao Zhang [a,b]

[a] State Key Laboratory of Applied Optics, Changchun Institute of Optics, Fine Mechanics and Physics, Chinese Academy of Sciences, Changchun, Jilin, 130033, China
[b] University of the Chinese Academy of Sciences, China
[c] Wuhan National Laboratory for Optoelectronics, Huazhong University of Science and Technology, Wuhan 430074, China
[d] Université Paris-Est, ESYCOM(EA2552), UPEMLV, ESIEE-Paris, CNAM F- 93162 Noisy le Grand, France

ARTICLE INFO

Keywords:
Metamaterial absorbers
Long wavelength infrared
Cavity modes

ABSTRACT

A wavelength-selective, ultrathin, broadband infrared metal–insulator–metal (MIM) absorber with multi-sized Ti–Ge cubes is proposed. By flexibly combining different sizes of Ti–Ge cubes, stacking upward and reasonably filling the border, all the resulting 3 structures that we propose show an average absorptivity of at least 90% over a wide spectral range in the infra-red, extending from 6. 3 μm to 14.8 μm. The absorptivity is further increased up to 99% when considering narrower spectral ranges such as 7.96-8.34 μm and 11.02-11.75 μm wavebands, which is superior than the previous work in long wavelength infrared band based on the MIM structure. Those characteristics vary depending on the 3 designs considered and studied in this work: single-layer structure, double-layer structure and modified structure. The intrinsic strong energy dissipation caused by highly lossy metal Ti (here Titanium) and excited low-Q cavity modes are key factors contributing to such efficient broadband absorption. The polarization and angle insensitivity are demonstrated by analysing the absorption performance with oblique incidences for both transverse electric wave (TE) and transverse magnetic wave (TM). Moreover, flexible combinations of different resonators allow trade-offs between the absorption bandwidth and the absorbance, which makes the operating waveband of the metamaterial absorber adjustable through proper design. The proposed broadband absorbers have many potential applications, including microbolometers, thermal emitters, and plasmonic sensors.

1. Introduction

Plasmonic metamaterial absorbers is attracting increased attention due to their excellent properties in the absorption of electromagnetic waves. Due to the strong absorption of light and the tunability of resonant wavelengths, plasmonic metamaterial absorbers have extensive applications in microbolometers [1,2], thermal emitters [3,4], energy harvesting [5–7], electromagnetic shielding [8,9] and sensors [10–13]. Various methods for designing metamaterial absorbers are emerging in an endless stream. A perfect metamaterial absorber that is based on the electromagnetic response in the microwave regime was the first absorber to be proposed [14]. This absorber consists of a top metallic layer with electric ring resonators (ERRs), a dielectric interlayer and a bottom metallic layer with cutting wires. A metamaterial absorber, which has metal–insulator–metal (MIM) cavities [15–17] and has been developed to subwavelength scales, can trap light beyond the diffraction limit.

The electromagnetic properties of the metamaterial absorber are described based on the effective parameters. The absorption of the target band can be maximized while minimizing unwanted reflections via engineering of these effective parameters to obtain impedance matching at the air–metamaterial absorber interface. However, the difficulty of obtaining broadband absorption at a large wavelength range considerably limits the application of the metamaterial absorber in various fields. An efficient method for expanding the bandwidth is to mix multiple resonators with adjacent resonant frequencies. Mixing multiple resonators in the same horizontal plane for the infrared frequency regime has been proven to enhance the absorption bandwidth [18,19]. In addition, the accumulation of multiple resonators on the vertical surface has been proven to increase the absorption bandwidth from near-infrared and visible ranges [20–22]. Utilizing metals with the high imaginary part of permittivity, such as tungsten and titanium, can also effectively improve the absorption bandwidth [4,23,24]. However, there are several disadvantages for such approach,

* Corresponding author.
E-mail address: liangzz@ciomp.ac.cn (Z. Liang).

https://doi.org/10.1016/j.optcom.2019.124948
Received 24 September 2019; Received in revised form 10 November 2019; Accepted 13 November 2019
Available online 15 November 2019

such as low average absorption efficiency, discrete resonant peaks and a complicated structure design [25–27].

Inspired by previous research on broadening the bandwidth of plasmonic metamaterial absorbers, we propose an MIM absorber specifically designed to operate in the mid and far infrared spectral ranges, constructed with multi-sized Ti–Ge cubes. By flexibly combining different sized resonators, a single-layer absorber appears to exhibit an average absorptivity greater than 90% from 6.26 μm to 13.55 μm, which represents better performance than the noble metal structure reported by Guo et al. (absorption greater than 90% from 7.8–12.1 μm) [22]. This finding is realized based on the excitation of the low-Q cavity modes induced by the metal–insulator–metal resonant cavity. The effects of the repeat period on the absorption performance of the individual resonators and the supercell are investigated to study the coupling effects within and out of each unit cell. Additionally, both the bandwidth and the average absorption are enhanced with an increase in the Ti–Ge bilayers due to the coupling of cavity modes in adjacent Ge layers. The double-layer and modified structure have an average absorptivity greater than 90% from 6.46 μm to 13.05 μm (and greater than 99% absorbance in the 7.11–11.08 μm waveband), as they exhibit excellent absorption and well merged resonant peaks. When the border is reasonably filled with a suitable-sized resonator, the absorption performance of the metamaterial absorber can be promoted. The proposed structures have the advantages of low cost and easy fabrication compared with previously reported studies, which employ noble metal and a complicated cell pattern [25–27]. This absorber structure will hold considerable potential in thermal emitters and microbolometer applications.

2. Modelling and simulation

2.1. Design principle and structure of the broadband absorber

Metamaterial absorbers are often designed as a metal–insulator–metal (MIM) structure that consists of a ground metal layer, a dielectric layer, and a top layer of periodically patterned metal. The MIM absorber follows a similar principle: The entire absorber can be regarded as a resonant cavity enclosed by magnetic walls that support cavity modes, which causes cavity modes-induced light absorption [28]. When incident light rips into the upper metal layer, the lower metal layer acts as a mirror that can reflect the surface plasmon excited at the lower metal–insulator interface. The destructive interference of the surface plasmon between the upper metal–insulator interface and the lower metal–insulator interface produces the cavity modes, which cause the trapping and absorbing of light. It is possible to maximize the absorption of the target band while minimizing unwanted reflections by engineering the geometric parameters of the MIM absorber to ensure sufficient energy coupling into the cavity modes. The thickness of the bottom metal layer is considerably larger than the skin thickness to prevent transmission. The thickness of the insulator layer should be smaller than the radiant wavelength to enable effective coupling of the surface plasmon between the upper metal–insulator interface and the lower metal–insulator interface. However, if the thickness of the insulator layer is too small, a high reflection will occur. A thinner top metal layer guarantees a less lossy cavity, whereas a thicker top metal layer implies a weaker coupling. Similar to a standard Fabry–Perot resonator, the resonance wavelength λ of MIM cavity can be adjusted by controlling the length of particle situated above the insulator film. The resonance condition for MIM resonant cavity can be written as [29]:

$$w\frac{2\pi}{\lambda}n_{cm} = m\pi - \varphi \tag{1}$$

where w is the length of particle, n_{cm} is the effective index of the cavity mode, m is an integer determining the order of a resonant cavity mode, and φ is the phase obtained by the reflection of the cavity mode at the resonator terminations. Considering only the fundamental mode ($m = 1$) and setting phase shift φ to zero, Eq. (1) can be transformed to:

$$wn_{cm} = \frac{\lambda}{2} \tag{2}$$

Thus, we can realize the ultra-high absorption in a broad spectral range in long wavelength Infrared band through designing the length of resonators.

In our design, an ultra-broadband absorber consists of a periodic array of multi-size titanium–germanium (Ti–Ge) cubes and a thick continuous Ti bottom layer, as shown in Fig. 1(a). Four resonators are integrated into a unit cell that can be separated into four equal parts; each resonator is placed in the centre of each section. The Ti–Ge cubes have four different widths of w_{1i} (i = 1, 2, 3, 4), including $w_{11} = 1.02$ μm, $w_{12} = 1.12$ μm, $w_{13} = 1.26$ μm, and $w_{14} = 1.40$ μm. The period of the unit cell is $p_1 = 3.72$ μm. Titanium (Ti), which exhibits lossy behaviour in the IR region, is selected as the metal material. The thickness of the bottom Ti layer is $t_1 = 0.25$ μm, which is considerably larger than the skin thickness to prevent transmission. Due to its transparent behaviour in the Near Infra Red (NIR), which indicates that absorption primarily occurs in the top metal layer, Germanium (Ge) is selected as the insulator material. The thickness of the insulator is $h = 1.04$ μm. The thickness of the top metal layer is $t_2 = 0.03$ μm. The complex dielectric constants of Ti are modelled by a Drude–Lorentz fitting to tabulate the experimental data [30], while Ge is considered to be lossless with a constant refractive index of 4.01.

Finite difference time domain (FDTD) method has been used to simulate the field distributions of ultra-broadband absorber. In the FDTD numerical simulations, the periodical boundary conditions are adopted in the x and y directions, and the perfectly matching layers (PML) are employed in the z direction. Absorption (A) is usually calculated by the formula $A = 1 - R - T$, where R and T represent reflection and transmission. Transmission equals zero since the thickness of the bottom metal layer is much larger than its skin depth to eliminate transmission, which indicates that $A = 1 - R$.

At first glance, the structure and principle of this proposed absorbers seem similar to some previous reports, especially the published one in [27]. However there also exist some obvious differences. Firstly, this paper aims to represent a method to gradually improve the absorption performance of the absorber, the absorber in [27] consists of three structural layers (four upper gold patches, four insulator patches, and a lower Au film); while the proposed absorbers here have three different structures, including the single-layered structure, double-layer structure and modified structure. The modified structure is more compact in structure and wider in bandwidth. The absorption performance is also improved with the increase of the fill factor. Secondly, the simulations of the field distributions and the coupling effects within and out of each unit cell are performed to demonstrate that the cavity modes around the dielectric patches excited by different sized resonators attribute to the broadband absorption, while that in [27] do not elaborate on resonance mechanism. Thirdly, the metallic material in [27] is Au and the working bandwidth is narrow, while the designed absorber here exhibits broadband and low-Q performance due to the highly lossy Ti.

2.2. Simulation results of the ultra-broadband single-layered plasmonic absorber

The property of the single resonator has been explored. The transmission line model and the simplified circuit model of the single resonator are presented in Fig. 1(b). According to the transmission line theory, the above metamaterial layer can be modelled as parallel resonant modes with coupling effects. Specifically, the top metamaterial layer can be regarded as LC and dipole resonant modes coupled by mutual inductance. The impedances of the LC and dipole resonant modes (Z_{LC} and Z_{dipole}) can be represented as [31]:

$$Z_{LC,dipole} = R_{LC,dipole} + \frac{2\varepsilon_i}{wc_{LC,dipole}(\varepsilon_r + 1)^2} + iwL_{LC,dipole}$$

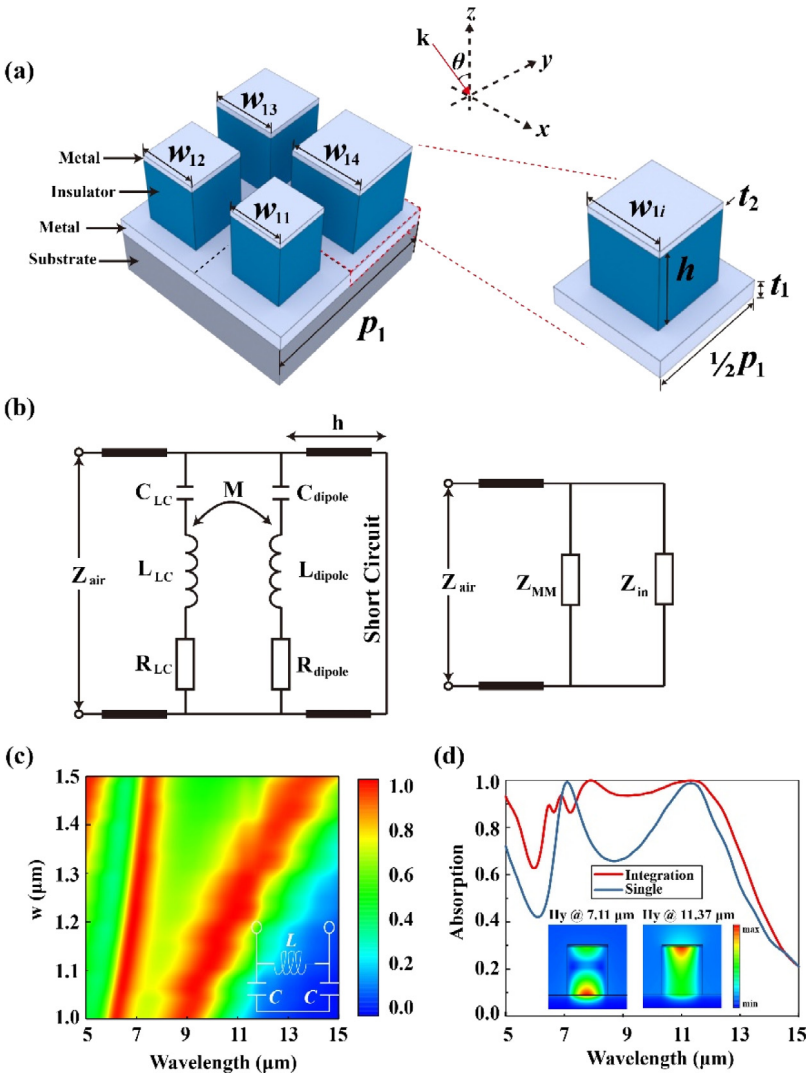

Fig. 1. (a) Schematic of the single-layered metamaterial absorber structure. (b) Demonstration of the width of the Ti–Ge cell cube (w) effects on the absorption performances of the single resonator with a single-layer structure at normal incidence. (c) Simulated absorption spectra of the integrated structure and the single resonator at normal incidence. The insets show the distribution of the normalized magnetic field Hy of the single resonator, in which the red colour and blue colour represent the maximum magnitude in the y direction and $-y$ direction, respectively.

$$+\frac{2}{iwc_{LC,dipole}(\varepsilon_r+1)} \tag{3}$$

where ε_r and ε_i are the real and imaginary part of the relative permittivity of the insulator, $R_{LC,dipole}$, $L_{LC,dipole}$, and $c_{LC,dipole}$ are the resistance, inductance, and capacitance values for the top metamaterial layer, respectively. The insulator layer is equivalent to a transmission line with a length equal to the thickness of the spacer and shorted by the ground plane, whose impedance can be described as:

$$Z_{in} = i\sqrt{\frac{\mu_d}{\varepsilon_d}}Z_0\tan(k_0\sqrt{\varepsilon_d\mu_d}d) \tag{4}$$

where Z_{in} is the impedance of the shorted transmission line, k_0 is the free space wave number, μ_d and $\varepsilon_d(\varepsilon_r+\varepsilon_i i)$ are the relative permeability and permittivity of the insulator, and d is the thickness of the insulator layer. Based on the equivalent circuit model shown in Fig. 1(b), the overall impedance of the metamaterial absorber can be written as:

$$Z_{MA} = \frac{Z_{MM}Z_{in}}{Z_{MM}+Z_{in}} \tag{5}$$

If the overall impedance of the absorber is perfectly matched with free space, the reflection will be reduced and perfect absorption can be achieved.

To explore the operating band of the individual resonators, the influence of the cell cube width (w) on the absorption spectra has been investigated. As shown in Fig. 1(c), each resonator has two discrete absorption peaks in the shorter wavelengths, which range from 6.10 μm to 7.70 μm, as well as in the longer wavelengths, which range from 8.60 μm to 13.90 μm. They also show better broadband absorption than noble metals because of the lossy Ti. Moreover, with an increase in the cell cube width (w), the structure develops by the tendency of a continuous sandwiched film, which produces a wider absorption bandwidth but a lower absorption. Thus, the distance between two absorption peaks increases as the cell cube width increases. The inset of Fig. 1c present the equivalent LC circuit, according to the LC circuit model, each of the two capacities is formed by the continuous bottom metal film and an upper or lower half of the cube. The capacitance C can be approximated by two capacitors, and the inductance L of the structure can be approximated by two parallel plates. Thus, the resonant frequency of the plasmonic absorber can be described as [32, 33]:

$$C = \frac{A\varepsilon_r\varepsilon_0 l^2}{2h} \tag{6}$$

$$L = \frac{B\mu_0 h}{2} \tag{7}$$

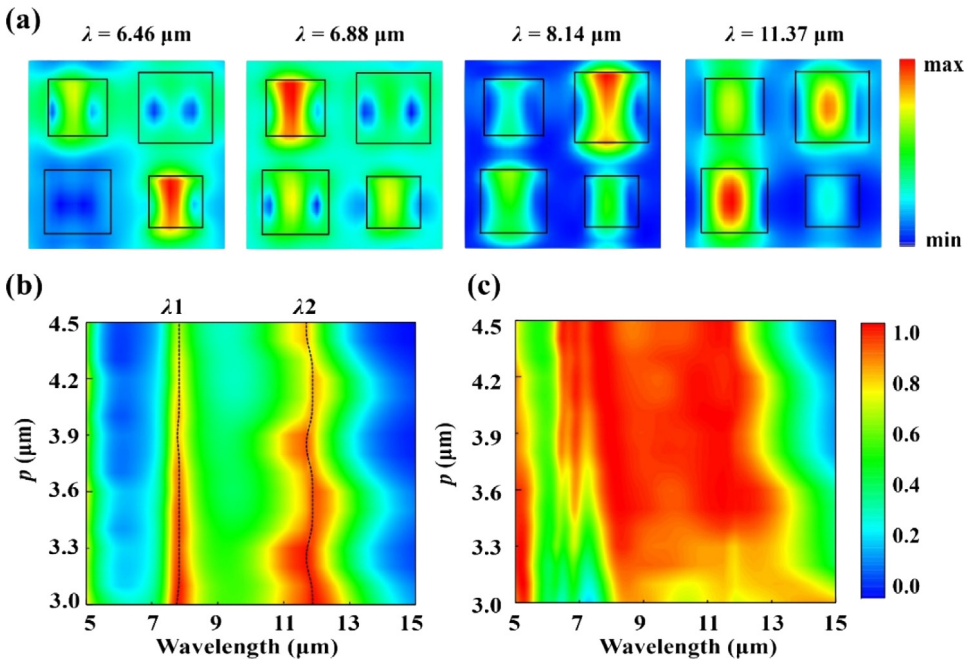

Fig. 2. (a) Magnetic field $|H|$ distributions (colour bar in the x-y plane) at different resonant frequencies in the dielectric layer of the single-layered metamaterial absorber. (b) Demonstration of the repeat period (p) effects on the absorption performance of the individual resonators at normal incidence. The dashed line represents the resonance wavelength. (c) Demonstration of the repeat period (p) effects on the absorption performance of the integrated structure at normal incidence.

$$f = \frac{1}{2\pi\sqrt{LC}} = \frac{c_0}{\pi\sqrt{AB\varepsilon_r}}\frac{1}{l} \tag{8}$$

where l represents the width of the cube, c_0 represents the speed of light in free space, h is the thickness of dielectric layer, and A and B are the numerical factors. This analysis indicates that the resonant frequency of the plasmonic absorber is inversely proportional to the width of the resonator, but exhibits little sensitivity to the change of separation distance h. The larger size resonators determine the resonant peaks of the longer wavelength, whereas the resonant peaks of the shorter wavelength are controlled by the smaller resonators. The resonator with a width of 1.30 μm is selected to study the resonance property, and two perfect absorption peaks (7.11 μm and 11.37 μm) arise in a separated location [Fig. 1(d)]. The magnetic field distribution of the x–z plane reveals that the magnetic field at the resonances is significantly enhanced and restricted to different regions of the dielectric layer. Based on the magnetic field distributions, two resonances comprise both of the cavity modes excited on the dielectric layer, which are attributable to the perfect absorption. However, two different cavity modes are observed in the magnetic field distribution. The magnetic field at 7.11 μm is strongly restricted above the interface between the bottom metal and the dielectric layer, which indicates that the constructive interference of coupled surface plasmons predominantly occurs here and implies that typical cavity modes contribute to high absorption. The magnetic field at 11.37 μm is actually confined below the interface between the top metal and the dielectric layer. Although the resonant cavity supports several cavity modes, only two modes can be effectively excited; they can be regarded as the symmetric and antisymmetric coupling of metal patches [34,35]. In this paper, only the symmetric mode is observed at normal incidence.

Four resonators are arranged in a unit cell. Considering the interaction between each resonant cavity, the structure must be optimized to obtain the broadband absorption of the target band. Absorption changes over the wavelength function plot are given in Fig. 1(d), which shows that the aligned structure has an average absorptivity that is greater than 90% from 6.26 μm to 13.55 μm and greater than 99% absorbance in the 7.96–8.34 μm and 11.02–11.75 μm wavebands. Four absorption peaks are located at the wavelengths λ_1 = 6.46 μm, λ_2 = 6.88 μm, λ_3 = 8.14 μm, and λ_4 = 11.37 μm in the absorption spectrum (see Table 1).

Table 1
Comparation with the single-layered absorber reported by Guo et al. [22]

	Dielectric materials	Metallic materials	Band of absorptance
Previous report	ZnS	Au	7.8–12.1 μm (over 90%)
Proposed absorber	Ge	Ti	6.26–13.55 μm (over 90%)

To further understand the resonance nature of the absorber and the mechanism of the absorption, the magnetic field distributions of each resonant wavelength are investigated, as shown in Fig. 2(a). Each resonance is caused by the interaction among the resonators with an adjacent size. The magnetic field distribution of the resonance at 6.46 μm is primarily gathered in patches with widths of w_1 and w_2. For the resonance at 6.88 μm, the magnetic distribution is focused on patches with widths of w_1, w_2, and w_3. Similarly, the magnetic distribution of the resonance at 8.14 μm (or 11.37 μm) is focused on patches with widths of w_3 and w_4 (or w_2, w_3, and w_4).

The magnetic field distributions imply that the resonance peaks correspond to the resonant cavity modes beneath patches of different sizes. The power loss of the cavity modes accumulates at resonances, where the energy is significantly coupled into the resonant cavity and subsequently converted into thermal energy, thus leading to perfect absorption. Note that the coupling effects between unit cells and the interaction between each resonant cavity mode are the main factors that influence the absorption of the absorber. Two sets of simulations are performed to study the coupling effects within and out of each unit cell on the properties of the absorption band. To reveal the effect of the coupling effects between each unit cell on absorption, we examined the influence on the absorption spectrum of the individual resonators with a change of the repeat period (p), as depicted in Fig. 2(b). It is clearly shown that the resonance in the shorter wavelength is much less perturbed by the variation of p. For the other resonance in the longer wavelength, the trend of this resonance undergoes a nonuniform distribution with an increase in p because of the fringe effect. As the resonant cavity enclosed by magnetic walls is not completely closed,

when the surface plasmon is reflected at the edges, an additional phase shift will occur due to the fringe effect. However, the cavity resonance frequencies are almost constant, which indicates that the coupling effects between each unit cell are negligible in this period range. Thus, the interaction among the resonant cavity modes dominates the absorption performance. To investigate the effect of the interaction between adjacent resonances on absorption, we also calculated the influence on the absorption spectrum of the supercell with a change in the repeat period (p), as shown in Fig. 2(c). The figure reveals that the absorption property of the absorber is sensitive to the repeat period. Specifically, the smaller p corresponds to the broader absorption bandwidth and the lower average absorptivity. To obtain a trade-off between the absorptivity and the absorption bandwidth, we selected the length of $p = 3.72$ μm. Consequently, the width of the resonator determines the position of the absorption peaks, and the repeat period has the effect of smoothly connecting adjacent bands.

2.3. Effects of material and incident-angle-insensitive on absorption performance

To highlight the advantages of introducing the cavity modes around the dielectric patches, all dielectric Ge patches in the structure are replaced by a continuous Ge layer. The thickness of each layer is consistent with the previously mentioned structure. The comparison of absorption spectra between Ge patches and Ge planar is presented in Fig. 3(a). The absorption spectra exhibit narrow resonances approximately 5.69 μm and 6.08 μm, which are considered to be the propagating surface plasmon (PSP) resonances between continuous Ti film and Ge spacer [36]. We observe that within the analysed wavelength area, the absorption of the Ge blocks structure is much better than the Ge planar structure because of the cavity mode enhancement. This finding corroborates that the cavity modes promote absorption in this broadband wavelength range. For comparison, all Ti in the structure is replaced by Au. Four sharp absorption peaks are observed in the range of 6-12 μm, which correspond to the respective cavity modes. The sharp absorption peaks indicate higher order cavity resonance is excited, resulting in highly-efficient narrowband absorption. This resonance exhibits higher Q factor compared to the fundamental cavity resonance as the fundamental cavity resonance has higher radiative loss [37]. The role of the top metal layer is to bind the incident light energy to the dielectric layer. When the rigorous coupling condition that is related to the permittivity and thickness of the metal is satisfied, the incident light will be perfectly absorbed by excitation of the resonant cavity modes. Thus, the top metal determines not only the Q factor of the cavity mode but the coupling strength between the incident light and the resonant cavity. In addition to the inherent dispersion properties of metals, the Q factor of the cavity mode in the structure of Au is relatively high, which indicates that the amplitude of the resonance near the resonance frequency is large, whereas the frequency range of the resonance is relatively small. Conversely, Ti, which is a highly lossy metal, produces low-Q resonances, which can effectively expand the operating bandwidth.

We next investigate the effect of some geometry parameters on the performance of this metamaterial absorber. As regards the impact of the thickness of the top metal, Fig. 4a indicate that a thinner top Ti ensures a less lossy cavity whereas a thicker one implies a weaker coupling. Ti, which is a highly lossy metal, helps to enhance the resistive effects, which in turn produces resonance with a relatively lower quality factor and effectively expands the operating bandwidth. In order to obtain a trade-off between the absorptivity of two main resonant wavelengths (λ_3, λ_4), we selected the thickness of $t_2 = 0.03$ μm. Fig. 4(b) and (c) represents the absorption spectra for different incident angle θ for the TM and TE polarizations at $\varphi = 0°$. The incident angle is swept by a step of 6° from 0° to 60°. For TM polarization, the absorption curve undergoes only a slight change and exhibits a high overall absorptivity when θ is less than 45°. With an increase in the incident angle, the ultra-broadband absorption response, which is attributed to the notion that the coupling strength between the incident wave and the cavity modes depends on the interaction between the horizontal component of the incident magnetic field and the magnetic field of the cavity modes[25]. The horizontal component of the incident magnetic field remains invariable with different θ, which indicates that the strength of the coupling and absorption slightly varies. Regarding TE polarization, the spectra exhibit an absorption dip in the investigated wavelength range as the incident angle increases, which causes a lower absorption efficiency and narrower bandwidth. This result is attributed to the notion that the horizontal component of the incident magnetic field decreases with an increase in θ, resulting in a decrease in the strength of the coupling and the absorption. The dashed line in Fig. 4 represents 80% absorption, which indicates excellent absorption performance for both TM and TE polarizations.

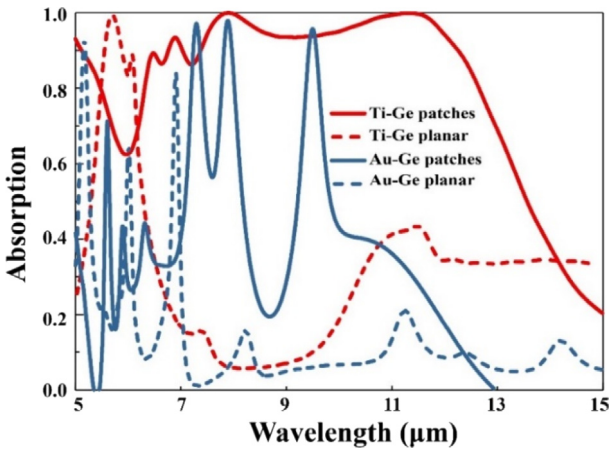

Fig. 3. Simulated absorption spectra of the Ti (Au)-Ge patches structure and the Ti (Au)-Ge planar structure at normal incidence.

3. Ultra-broadband dual-layered plasmonic absorber

Increasing the number of layers of upward stacked resonators can further enhance absorption and expand the bandwidth of the metamaterial absorber, including the microwave metamaterial absorber [38] and the THz metamaterial absorber [39]. Wu et. Al [40] reported that the infrared spectrum achieved a wavelength range from the entire visible region and most of the solar infrared region with high absorption. The hybridization of various resonances in the operating band can be achieved by stacking the number of metal–insulator pairs. A double-stack metamaterial absorber is described in Fig. 5(a). Two pairs of alternating Ti–Ge cubes of four different sizes are assembled in one unit cell. With the numerical parameter sweep, the final optimal geometrical parameters are provided as follows: the period of the unit cell is $p_2 = 6$ μm; and the thicknesses of the Ti–Ge-Ti–Ge-Ti layers from top to bottom are 0.04 μm, 0.66 μm, 0.025 μm, 0.92 μm and 0.25 μm, respectively. Two pairs of Ti–Ge cubes have the same widths of w_{2i} (i = 1, 2, 3, 4), including $w_{21} = 1.10$ μm, $w_{22} = 1.26$ μm, $w_{23} = 1.34$ μm, and $w_{24} = 1.52$ μm.

Similarly, we have investigated the property of the individual resonators. The influence of the cell cube width (w) on the absorption spectra is shown in Fig. 5(b). As depicted in Fig. 5(b), two absorption peaks of a single resonator with a double-layered structure are effectively merged and forms a continuous absorption band. The double-layer resonator with a width of 1.30 μm is selected to reveal the broadband absorption, two absorption peaks ($\lambda_1 = 7.90$ μm, $\lambda_2 = 9.62$ μm arise in close position, which improves the overall absorption compared with the single-layer structure. The magnetic field distributions of x–z plane show the analogous field profile with the cavity

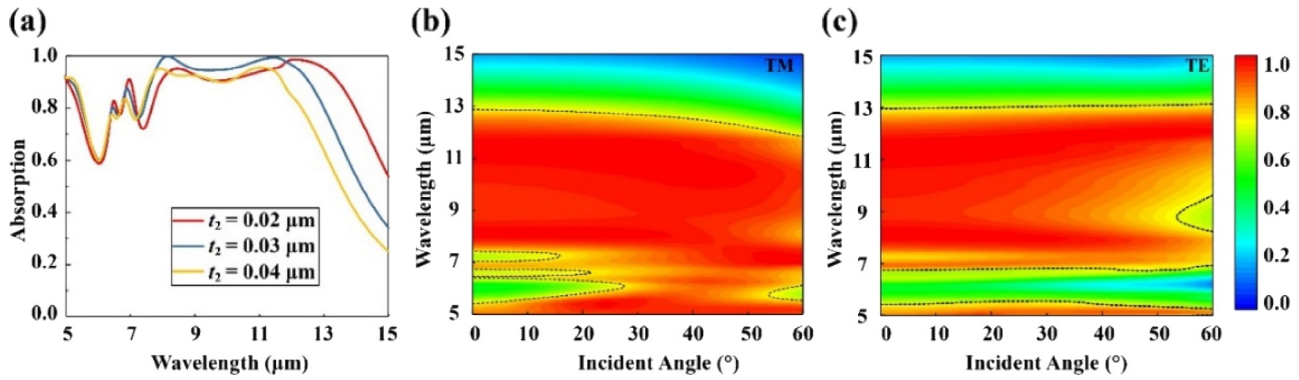

Fig. 4. The influence of geometric parameters on the performance of the absorber (a) the thickness of the top metal; (b) TM and (c) TE polarization. The dashed line represents the contour line with an absorption magnitude of 80%.

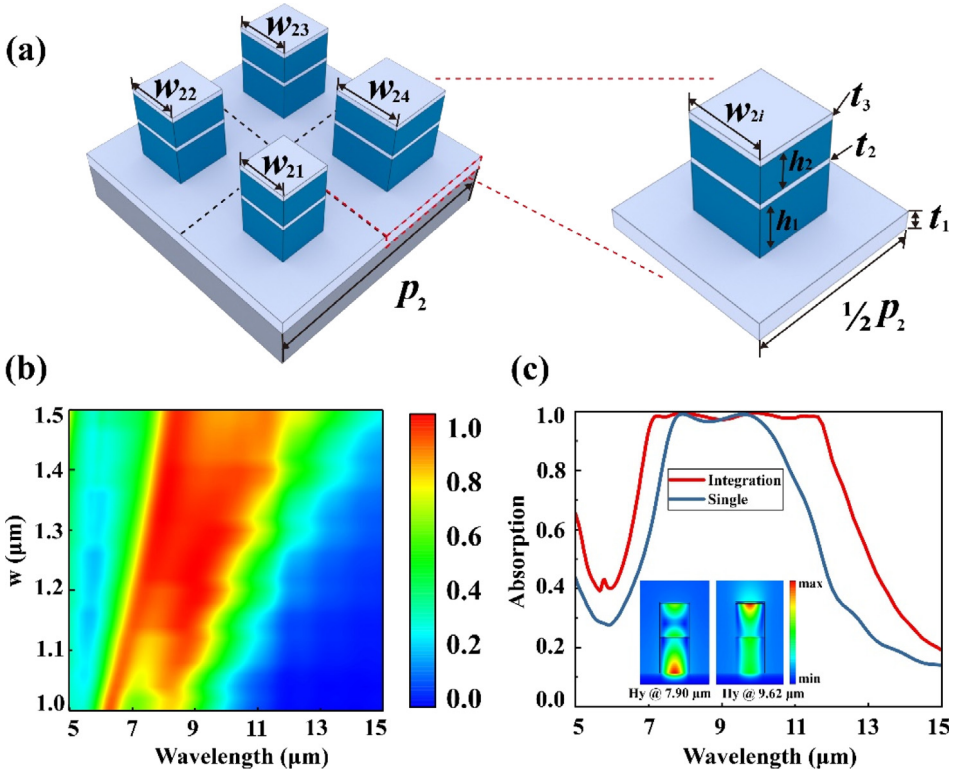

Fig. 5. (a) Schematic of the double-layer metamaterial absorber structure. (b) Demonstration of the width of the Ti–Ge cell cube (w) effects on the absorption performances of single resonator with double-layer structure at normal incidence. (c) Simulated absorption spectra of the integrated and single double-layer metamaterial absorber structure at normal incidence. The insets show the distribution of the normalized magnetic field Hy of the single double-layer resonator, in which the red colour and blue colour represent the maximum magnitude in the y direction and -y direction, respectively.

modes in the single-layer structure, which implies that two different cavity modes are excited in the metamaterial absorber. In addition, the two resonances originate from the hybridization between the cavity mode in the upper Ge layer and the cavity mode in the lower Ge layer, which enhances the bandwidth and absorption. According to the coupled oscillator model, the proposed structure can be interpreted as a series of harmonic oscillators driven by external forces. The oscillators represent resonant cavity modes in the Ge layers; with the increment of Ti–Ge bilayers, the number of absorption peaks increases due to the resonant cavity modes coupling between neighbouring Ge layers. Consequently, these peaks are combined to form broadband absorption. The absorption spectrum of the integrated structure is displayed in Fig. 5(c). In the figure, merged resonant peaks and more than 90% absorbance are observed in the interval from 6.46 μm to 13.05 μm. In addition, a nearly perfect absorbance (more than 99%) is obtained from 7.11 μm to 11.08 μm.

The absorption properties of a bilayer structure are better than the absorption properties of with a single-layer structure. Since the cavities are assembled in a compact unit cell, degeneration between two continuous peaks shrinks the operating bandwidth. To compensate for an insufficient absorption of a long wavelength, a new resonator has been introduced to the structure to rationalize the space of one unit cell. The principle that the resonant frequency of a plasmonic absorber is inversely proportional to the width of the resonator, which suggests that a resonator with a relatively large width should be selected. The interaction between adjacent resonators should be weakened while taking advantage of the coupling effects between each unit cell. An appropriate period is chosen to make the interaction between the resonators negligible to the total absorption performance of the metamaterial absorber. In this case, the length of the cavity has an important role in the absorption of the metamaterial absorber; the identical width but different displacement of the resonators can provide a similar

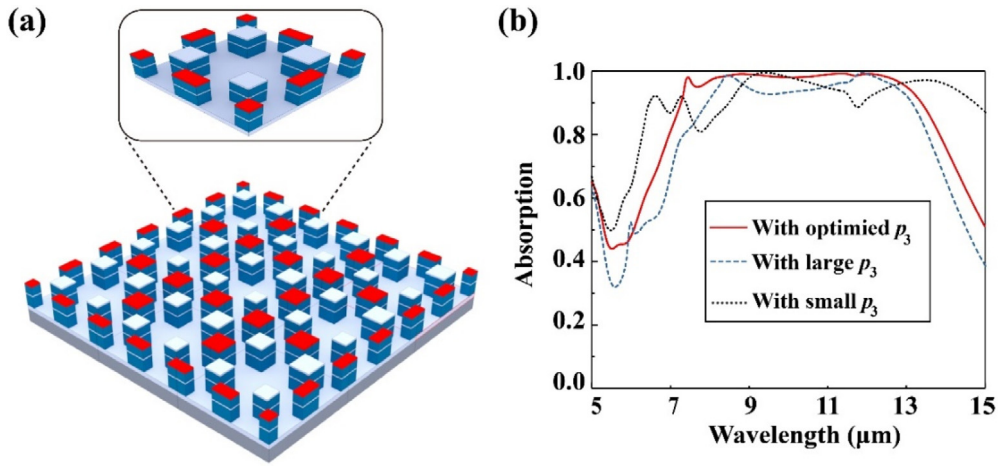

Fig. 6. (a) 3 × 3 array of the Ti–Ge cube metamaterial absorber structure. (b) Simulated absorption spectra with different repeat period (p_3).

Table 2
Comparation with the double-layered absorber reported by Guo et al. [22]

	Dielectric materials	Metallic materials	Band of absorptance
Previous report	ZnS/Al_2O_3	Au	5.3-13.7 μm (over 80%)
Proposed absorber	Ge	Ti	6.3–14.6 μm (over 90%) 8–14 μm (over 97%)

absorption. The typical combination is shown in Fig. 6(a): rectangular resonators with a length of w_4 and a width of $1/2w_4$ are introduced to the middle of four frames of a unit cell. To obtain a wider bandwidth, we suggest that patch resonators with a width of $1/2w_5$ be arranged at four corners of a unit cell, which may improve the performance of the metamaterial absorber (see Table 2).

As shown in Fig. 6(a), suitably sized resonators are introduced to the border of a unit cell. The geometrical parameters after optimization are provided, i.e., p_3 = 7.4 μm, w_{31} = 1.10 μm, w_{32} = 1.26 μm, w_{33} = 1.34 μm, w_{34} = 1.51 μm, and w_{35} = 1.60 μm; and the thicknesses of the Ti–Ge-Ti–Ge-Ti layers from top to bottom are 0.026 μm, 0.67 μm, 0.026 μm, 0.95 μm and 0.25 μm, respectively. The red line in Fig. 6(b) represents the absorption spectra of the multi-sized unit cells, which implies that this combination has an average absorption that exceeds 90% within the range of 6.3 μm to 14.6 μm. We also examined the influence on absorption with a change in the repeat period (p). The relative smaller p indicates a larger filling factor, and the structure exhibits the tendency of a continuous sandwiched film, which causes a broader absorption bandwidth and lower average absorptivity. Conversely, the structure with a relatively smaller filling factor shows an intensive cavity mode resonance, and the absorbance increases at the expense of an increase in p. This flexible combination can satisfy the desired bandwidth and absorbance. When a wide absorption bandwidth is not required, the number of identical sized resonators can be selected to achieve high absorption. Similarly, broadband absorption can be achieved by sacrificing the absorption efficiency of a certain band. Moreover, this type of plasmonic absorber achieves a nearly perfect absorbance (more than 97%) in the 8-14 μm waveband, which is important for infrared devices, such as microbolometer and quantum dot infrared photodetectors. The 8-14 μm waveband represents the long-wave infrared atmospheric windows, which provide working bands for detectors without interferences from dust, water vapour, or other atmospheric influences. In addition, this waveband has been described as the thermal imaging region, where sensors can obtain a completely passive image of objects with temperatures that are slightly higher than room temperature [41].

4. Conclusion

In conclusion, an ultrathin broadband infrared MIM absorber with multi-sized Ti–Ge cubes has been proposed. The wavelength-selective metamaterial absorber can be realized by flexibly combining different sizes of Ti–Ge cubes, increasing the number of upward layers and reasonably filling the border. The single-layer structure, double-layer structure and modified structure have an average absorptivity greater than 90% from 6.26 μm to 13.55 μm (greater than 99% absorbance in the 7.96–8.34 μm and 11.02–11.75 μm waveband), 90% from 6.46 μm to 13.05 μm (greater than 99% absorbance in the 7.11–11.08 μm waveband) and 90% from 6.3 μm to 14.8 μm (greater than 97% absorbance in the 7.2–14.09 μm waveband), respectively. The strong energy dissipation caused by highly lossy metal Ti and the excited low-Q resonance cavity modes contribute to this broadband efficient absorption. In addition, the structure has the advantages of low cost and easy fabrication compared with those discussed in previously reported studies that use noble metal and a complex manufacturing process. This flexible combination can satisfy the desired bandwidth and absorbance. If a wide absorption bandwidth is not required, a certain number of identical resonators can be selected to achieve high absorption. Certainly, the operating band can be tuned to other frequency bands. This broadband absorber has many potential applications in microbolometers, thermal emitters, and plasmonic sensors.

CRediT authorship contribution statement

Yi Luo: Conceptualization, Datacuration, Writing-originaldraft, Writing - review & editing. **Dejia Meng:** Datacuration, Writing - review & editing . **Zhongzhu Liang:** Conceptualization, Funding acquisition, Supervision, Writing - review & editing. **Jin Tao:** Writing - original draft, Writing - review & editing. **Jingqiu Liang:** Writing - original draft, Writing - review & editing. **Changhong Chen:** Writing - original draft, Writing - review & editing. **Jianjun Lai:** Writing - original draft, Writing - review & editing. **Tarik Bourouina:** Writing - review & editing. **Yuxin Qin:** Writing - review & editing. **Jinguang Lv:** Writing - review & editing. **Yuhao Zhang:** Writing - review & editing.

Acknowledgements

This study was supported by the National Natural Science Foundation of China (Grant Numbers 61735018, 61376122 and 61805242), Excellent Member of Youth Innovation Promotion Association CAS, China (Grant Numbers. 2014193), Scientific and Technological Development Project of Jilin province, China (Grant Numbers. 20170204077GX), Leading Talents and Team Project of Scientific and

Technological Innovation for Young and Middle-aged Groups in Jilin Province (20190101012JH), Independent fund of State Kay Laboratory of Applied Optics, China, Overseas Students Science and Technology Innovation and Entrepreneurship Projects, China, Project of CIOMP-Duke Collaborative Research, China, Project of CIOMP-Fudan University Collaborative Research, China.

References

[1] T. Maier, H. Brueckl, Multispectral microbolometers for the mid-infrared, Opt. Lett. 35 (22) (2010) 3766–3768.
[2] J.-Y. Jung, K. Song, J.-H. Choi, J. Lee, D.-G. Choi, J.-H. Jeong, D.P. Neikirk, Infrared broadband metasurface absorber for reducing the thermal mass of a microbolometer, Sci. Rep. 7 (1) (2017) 430.
[3] Y. Gong, Z. Wang, K. Li, L. Uggalla, J. Huang, N. Copner, Y. Zhou, D. Qiao, J. Zhu, Highly efficient and broadband mid-infrared metamaterial thermal emitter for optical gas sensing, Opt. Lett. 42 (21) (2017) 4537–4540.
[4] Z. Li, L. Stan, D.A. Czaplewski, X. Yang, J. Gao, Wavelength-selective mid-infrared metamaterial absorbers with multiple tungsten cross resonators, Opt. Lett. 26 (5) (2018) 5616–5631.
[5] C.-F. Guo, T. Sun, F. Cao, Q. Liu, Z. Ren, Metallic nanostructures for light trapping in energy-harvesting devices, Light: Sci. Appl. 3 (2014) 161.
[6] S. Han, J.-H. Shin, P.-H. Jung, H. Lee, B.J. Lee, Broadband solar thermal absorber based on optical metamaterials for high-temperature applications, Adv. Opt. Mater. 4 (8) (2016) 1265–1273.
[7] F.O. Alkurt, O. Altintas, M. Ozakturk, M. Karaaslan, O. Akgoland, E. Unal, C. Sabah, Enhancement of image quality by using metamaterial inspired energy harvester, Phys. Lett. A 9 (2019) 126041.
[8] M. Esen, İ. Ilhan, M. Karaaslan, R. Esen, Investigation of electromagnetic and ultraviolet properties of nano-metal-coated textile surfaces, Appl. Nanosci. (2019) 2190–5517.
[9] M. Ozturk, O. Akgol, U. KorkutSevim, M. Karaaslan, M. Demirci, E. Unal, Experimental work on mechanical, electromagnetic and microwave shielding effectiveness properties of mortar containing electric arc furnace slag, Constr. Build. Mater. 165 (2019) 58–63.
[10] J. Grant, Y. Ma, S. Saha, A. Khalid, D.R. Cumming, Polarization insensitive broadband terahertz metamaterial absorber, Opt. Lett. 17 (36) (2011) 3476–3478.
[11] C. Wu, A.B. Khanikaev, R. Adato, N. Arju, A.A. Yanik, H. Altug, G. Shvets, Fano-resonant asymmetric metamaterials for ultrasensitive spectroscopy and identification of molecular monolayers, Nature Mater. 11 (1) (2011) 69–75.
[12] Y.I. Abdulkarim, L. Deng, M. Karaaslan, M. Demirci, E. Unal, Determination of the liquid chemicals depending on the electrical characteristics by using metamaterial absorber based sensor, Chem. Phys. Lett. 732 (2019) 136655.
[13] M. Bakır, Ş. Dalgaç, M. Karaaslan, F. Karadağ, O. Akgol, E. Unal, T. Depçi, C. Sabah, A comprehensive study on fuel adulteration sensing by using triple ring resonator type metamaterial, J. Electrochem. Soc. 166 (12) (2019) B1044–B1052.
[14] N.I. Landy, S. Sajuyigbe, J.J. Mock, D.R. Smith, W.J. Padilla, Perfect metamaterial absorber, Phys. Rev. Lett. 100 (20) (2008) 207402.
[15] P. Zhu, L.J. Guo, High performance broadband absorber in the visible band by engineered dispersion and geometry of a metal–dielectric-metal stack, Appl. Phys. Lett. 101 (24) (2012) 241116.
[16] P. Feng, W.-D. Li, W. Zhang, Dispersion engineering of plasmonic nanocomposite for ultrathin broadband optical absorber, Opt. Express 23 (3) (2015) 2328–2338.
[17] S.A. Dereshgi, Z. Sisman, K. Topalli, A.K. Okyay, Plasmonically enhanced metal–insulator multistacked photodetectors with separate absorption and collection junctions for near-infrared applications, Sci. Rep. 7 (2017) 42349.
[18] X. Liu, T. Tyler, T. Starr, A. Starr, N. Jokerst, W. Padilla, Taming the blackbody with infrared metamaterials as selective thermal emitters, Phys. Rev. Lett. 107 (2011) 045901.
[19] W. Ma, Y. Wen, X. Yu, Broadband metamaterial absorber at midinfrared using multiplexed cross resonators, Opt. Express 21 (2013) 30724–30730.
[20] B. Adomanis, C. Watts, M. Koirala, X. Liu, T. Tyler, K. West, T. Starr, J. Bringuier, A. Starr, N. Jokerst, W. Padilla, Bi-layer metamaterials as fully functional near-perfect infrared absorbers, Appl. Phys. Lett. 107 (2015) 021107.
[21] J. Tian, H. Luo, Q. Li, X. Pei, K. Du, M. Qiu, Near-infrared super-absorbing all-dielectric metasurface based on single-layer germanium nanostructures, Laser Photon. Rev. 12 (2018) 1800076.
[22] W. Guo, Y. Liu, T. Han, Ultra-broadband infrared metasurface absorber, Opt. Lett. 35 (24) (2016) 20586–20592.
[23] W. Wang, Y. Qu, K. Du, S. Bai, J. Tian, M. Pan, H. Ye, M. Qiu, Q. Li, Broadband optical absorption based on single-sized metal–dielectric-metal plasmonic nanostructures with high-ϵ metals, Appl. Phys. Lett. 110 (2017) 101101.
[24] K. Aydin, V. Ferry, R. Briggs, H. Atwater, Broadband polarization independent resonant light absorption using ultrathin plasmonic super absorbers, Nature Commun. 2 (2011) 517.
[25] C. Koechlin, P. Bouchon, F. Pardo, J. Jaeck, X. Lafosse, J.-L. Pelouard, R. Haidar, Total routing and absorption of photons in dual color plasmonic antennas, Appl. Phys. Lett. 99 (24) (2011) 241104.
[26] Y. Cui, J. Xu, K.H. Fung, Y. Jin, A. Kumar, S. He, N.X. Fang, A thin film broadband absorber based on multi-sized nanoantennas, Appl. Phys. Lett. 99 (25) (2011) 253101.
[27] P. Bouchon, C. Koechlin, F. Pardo, R. Haïdar, J.L. Pelouard, Wideband omnidirectional infrared absorber with a patchwork of plasmonic nanoantennas, Opt. Lett. 37 (6) (2012) 1038–1040.
[28] X. Ming, Q. Tan, Design method of a broadband wide-angle plasmonic absorber in the visible range, Plasmonics 12 (1) (2017) 117–124.
[29] M.G. Nielsen, D.K. Gramotnev, A. Pors, O. Albrektsen, S.I. Bozhevolnyi, Continuous layer gap plasmon resonators, Opt. Express 19 (20) (2011) 19310–19322.
[30] E.D. Palik, Handbook of Optical Constants of Solids, Academic, 1998.
[31] A.K. Azad, A.J. Taylor, E. Smirnova, J.F. O'Hara, Characterization and analysis of terahertz metamaterials based on rectangular split-ring resonators, Appl. Phys. Lett. 92 (1) (2008) 011119.
[32] J. Zhou, E.N. Economon, T. Koschny, C.M. Soukoulis, Unifying approach to left-handed material design, Opt. Lett. 31 (2006) 3620.
[33] Y. Ye, Y. Jin, S. He, Omnidirectional, polarization-insensitive and broadband thin absorber in the terahertz regime, J. Opt. Soc. Amer. B 27 (3) (2010) 498–504.
[34] R. Filter, J. Qi, C. Rockstuhl, F. Lederer, Circular optical nanoantennas: an analytical theory, Phys. Rev. B 85 (2012) 125429.
[35] F. Minkowski, F. Wang, A. Chakrabarty, Q.-H. Wei, Resonant cavity modes of circular plasmonic patch nanoantennas, Appl. Phys. Lett. 104 (2014) 021111.
[36] J. Cong, Z. Zhou, B. Yun, L. Lv, H. Yao, Y. Fu, N. Ren, Broadband visible-light absorber via hybridization of propagating surface plasmon, Opt. Lett. 41 (9) (2016) 1965–1968.
[37] F. Ding, J. Dai, Y. Chen, J. Zhu, Y. Jin, S.-I. Bozhevolnyi, Broadband near-infrared metamaterial absorbers utilizing highly lossy metals, Sci. Rep. 6 (2016) 39445.
[38] F. Ding, Y. Cui, X. Ge, Y. Jin, S. He, Ultra-broadband microwave metamaterial absorber, Appl. Phys. Lett. 100 (10) (2012) 103506.
[39] S. Liu, H. Chen, T.J. Cui, A broadband terahertz absorber using multi-layer stacked bars, Appl. Phys. Lett. 106 (15) (2015) 151601.
[40] D. Wu, Y. Liu, Z. Xu, Z. Yu, L. Yu, L. Chen, C. Liu, R. Li, R. Ma, J. Zhang, H. Ye, Numerical study of the wide -angle polarization- independent ultra-broadband efficient selective solar absorber in the entire solar spectrum, Sol. RRL. 1 (7) (2017) 1700049.
[41] Y. Luo, Z. Liang, D. Meng, J. Tao, J. Liang, C. Chen, J. Lai, Y. Qin, J. LV, Y. Zhang, Ultra-broadband and high absorbance metamaterial absorber in long wavelength infrared based on hybridization of embedded cavity modes, Opt. Commun. 448 (1) (2019) 1–9.